STUDY ON VORTEX CURRENT IN STRAIT WITH REMOTE-SENSING

by

Sotoaki Onishi
Professor of Civil Engineering Department,
Science University of Tokyo, Noda-Chiba, Japan

Tsukasa Nishimura
Researcher of Civil Engineering Department,
Science University of Tokyo, Noda-Chiba, Japan

INTRODUCTION

With rapid increases of industrial activity in present time, water pollution in the coastal environment has become an urgent problem to cope with. This problem is especially serious in enclosed bays or inland seas. Hydrodynamic character of the strait connecting the inland sea to the open ocean must be understood well in order to analyse the diffusion of pollutants in the inland sea, because its character determine boundary conditions in the mathematical models of the water pollution problem. So far however, it is seemed that the main efforts exerted by coastal engineers have concentrated mainly on the development of mathematical models, lacking satisfactory knowledge of the boundary conditions through field measurements. One reason of this state is resulted from the fact that the relating phenomena in the field are of too large scale, in general, to perform the field measurements.

Connecting with this point, the authors present in this paper, that remote-sensing technology is very useful to get information of the hydrodynamical phenomena occuring in the water body around the strait. To show the above, the authors selected as an object of the study , Naruto Strait in the Seto Inland Sea, which is world famous for the existence of rapid tidal currents and dynamic vortices. Remote-sensing data both from the airplanes and from a space satellite Landsat are analysed with the aid of theoretical considerations and hydraulic model tests to disclose the behavior of the vortices of various scales and the roles of them in the sea water mixing phenomena at the strait.

1. VORTEX DISTRIBUTION IN NARUTO STRAIT

Naruto Strait, being well known with the existence of dynamic vortices, is located between Shikoku and Awaji Island in Japan (Fig-1). Fig-2 is an aerophoto of the Naruto Strait. The left side on the figure is Harima Sea forming a part of the Seto Inland Sea and the right side is Kii Channel leading to the Pacific Ocean. The width of the Naruto Strait is, as shown in Fig-3 (a), contracted by shoals stretching out from both Oge Island in Shikoku and Tozaki Headland in Awaji Island. The most contracted section in the strait has V-shaped configuration as indicated in Fig-3 (b), in which the water surface is of 1,100m width, and the maximum depth is more than 80m. Each of the tidal levels in the Harima Sea and the Kii Cannel turns reversly with the period of 12hours, Fig-1 Location of the Naruto Strait

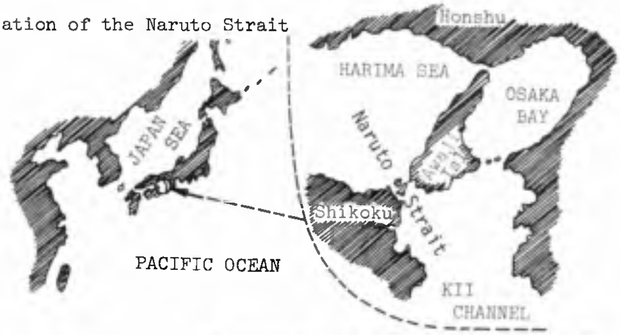

Fig-2 Aerophoto of the Naruto Strait

0 500m

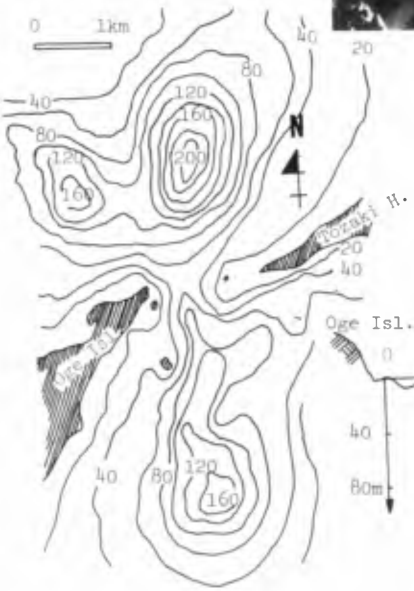

Fig-3 Topography of the Naruto Strait

(a) plan view

(b) section view of the Naruto Strait

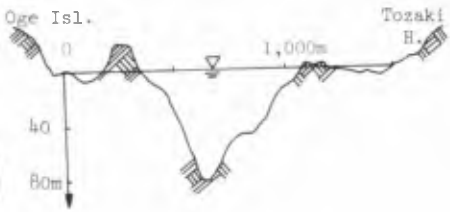

producing rapid tidal currents, the maximum velocity of which is about 10 knot, the dynamic vortices that are asserted roughly into coherent vortices along the free boundary layers leaving from both of the headlands, and vortex-pairs of large scale as schematically indicated in Fig-4. On the Fig-2, one can see the dynamic coherent vortices behind the headlands. Fig-5 shows the closer view of the coherent vortices. On the figure, one can see some aspects of the process through which rather smaller vortices amalgamate into the coherent vortices of larger size.

The authors investigated hydraulic character of these vortices through two different ways of field survey. The first of those is the remote-sensing with aero-photography, main purpose of which is to study the hydraulic character of the coherent vortices along the free boundary layer. The second way of the survey is the remote-sensing by Landsat, the purpose of which is to disclose the distribution of the larger scale vortex-pairs appearing as a result of amalgamation of the small scale coherent vortices.

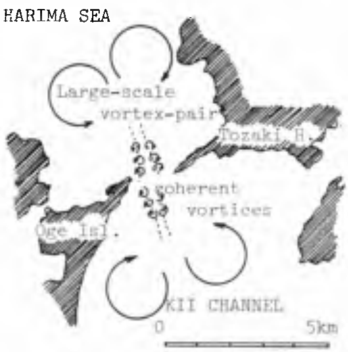

Fig-4. Vortices associated with tidal current at Naruto Strait

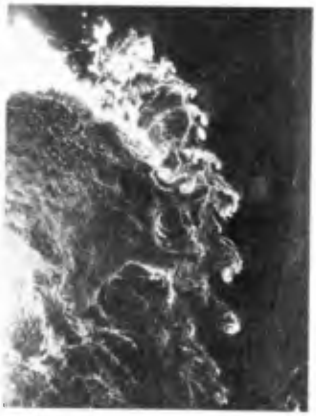

Fig-5 Amalgamation process of small scale vortices to larger scale ones

(aerophoto from 300m altitude)

0 100m

2. INVESTIGATION OF COHERENT VORTICES THROUGH SOLID AERO-PHOTOGRAPHY

2-1 Field observation

The aero-photographic surveys at Naruto Strait were done using a pair of airplanes at the altitude of 800m under the flood tide conditions of spring and autumn in 1978. Several series of aerophotos of the strait were synchronously obtained by the pair of airplanes at 3 sec time intervals and analysed through a stereoscope to map the hydraulic character of the strait such as unevenness of the water surface, direction of the tidal current, distribution of the vortices along the free boundary layers, upwelling currents and so on. Fig-6 is an example of the map gained. One of the interesting aspect is the existence of upwelling region, indicated by dotted line on the figure, on the water surface in the region opposite to the tidal current. Relations between the vortices and the upwelling current will be discussed in the paragraph 2-4 later.

Another example of the results obtained through the field survey is Fig-7 which represents the unevenness of the water surface. This figure was yielded through the solid aerophoto and will be used in the estimation of the vortex strength as described below.

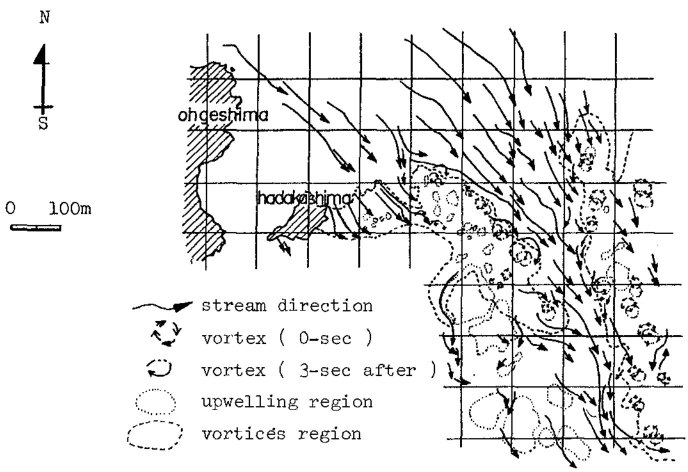

Fig-6 Distribution of tidal currents, coherent vortices and upwelling regions

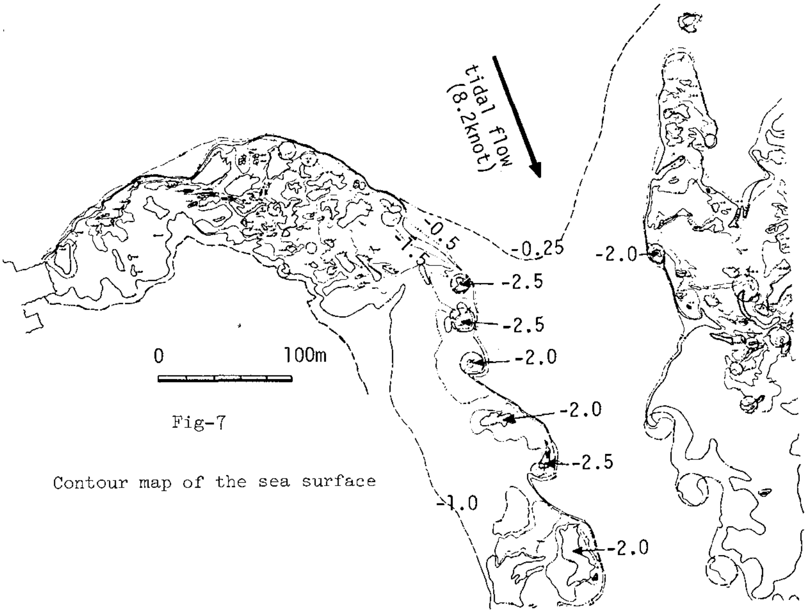

Fig-7

Contour map of the sea surface

2-2 Strength of the Coherent Vortices

From hydrodynamical view point, the vortex strength Γ in the practical sea water region with large scale such as the strait is quite an interesting subject to study. But, because of the unsteadiness as well as huge scale of the related hydraulic phenomena, the field measurement of the vortex strength by means of conventional instruments shall be considerably difficult. In this respect, the remote-sensing technology by the airplane and/or the satellite Landsat is quite useful. Here, authors present several ways to estimate the vortex strength with the data obtained through the remote-sensing.

(1) Estimation on the basis of " Rankine-Vortex " model

By applying the Rankine-vortex model to the individual vortex on the Fig-7, the vortex strength Γ_1 can be estimated by

$$\Gamma_1 = 2\pi R \sqrt{g \Delta h} \tag{1}$$

where R : vortex radius, g : acceleration of the gravity
Δh : concavity of the water surface on the vortex axis

On the Fig-7, we can obtain Δh directly and R by the fact that the vortex radius is equal to the radius of the contourline of the concavity of $\Delta h/2$.

(2) Estimation on the basis of "Concept of vorticity flux conservation"

Refering to Fig-8 and assuming that the strength of vorticity generated at the point P will be preserved during transport to the downstream direction along the free boundary layer, the vorticity flux passing through the control section I in a unit time can be estimated as follows.

Volume flux of the fluid passing through an element of thickness dy in the unit time is u dy , where u is the velocity in the direction normal to the y-axis. The vorticity ω in the fluid of unit volume is

$$\omega = du / dy$$

therefore, the vorticity flux ω_{flux} passing through the control section I becomes

$$\omega_{flux} = \int_{-\infty}^{\infty} u \, dy = \int_{-\infty}^{\infty} \frac{du}{dy} u dy = \frac{1}{2} (U_1^2 - U_2^2) \qquad (2)$$

where, U_1 and U_2 are the velocities above and below the boundary layer as shown in Fig-8 (a) respectively. With assumption that the free boundary layer consists of the group of coherent vortices, each of which is distributed in a constant space interval of b and posseses a shifting velocity of C as shown in Fig-8(b), the strength of each coherent vortex Γ_2 becomes

$$\Gamma_2 = \omega_{flux} \cdot \tau = \frac{1}{2} (U_1^2 - U_2^2) \frac{b}{C} \qquad (3)$$

where, τ = b/C is the average shedding period of the vortices.

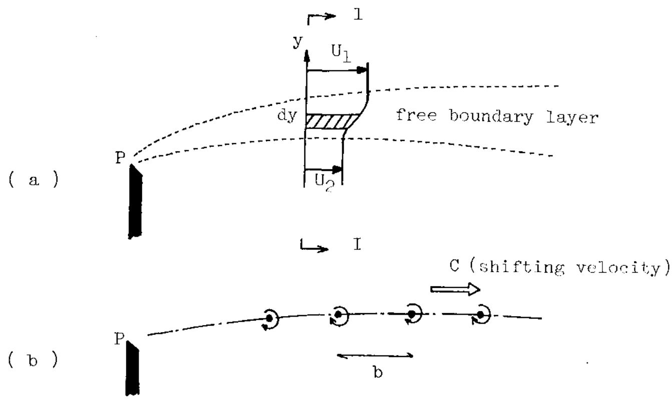

Fig-8 Concept of vorticity flux conservation

(5) The sediment moving directly onshore from the Swash Bar, Q(6) can split into longshore components Q(7) or Q(8) and Q(8) can be broken down into its ebb and flood constituents.

Hence : Q(6) = Q(7) + Q(8); Q(8) = Q(8E) + Q(8F)

(6) Prior to jetty construction North Beach was relatively stable i.e. Q(5) = Q(4) + Q(7).

6.2 Functional Relationships

(1) It was assumed that 90% of the flood tide sediment transport took place via the swash bar and inshore gutter i.e. Q(3) = 0.1 Q(8F).

(2) The ebb and flood sediment transport potential against the inside of the northern training wall was calculated from tidal current measurements assuming transport potential was proportional to the cube of the velocity (Maddock 1969). This indicated that the recycled ebb tide constituent of the inshore gutter sand feed was approximately half the flood tide constituent, therefore

Q(8E) = 0.3 Q(8)

(3) The application of the CERC formula to determine the net littoral transport along North Beach, Q(5), and the onshore transport on the Swash Bar, Q(2), was discussed in Section 3.4 where it was argued:

Q(2) = 10 Q(5)

6.3 Calculated Values

A number of the model elements where known or estimated viz:

(1) Q(1) = 20,000 m^3 p.a. (See section 3.3)

(2) Because currents in the inshore gutter were always inlet directed (Section 3.2) it was assumed that all sand feed would be inlet directed i.e. Q(7) = 0

(3) Q(9) = 50,000 m^3 p.a. (Section 3.1)

(4) Q(12) = 200,000 m^3 p.a. (Section 3.1)

(5) Q(11) = 150,000 m^3 p.a. (Section 3.1)

(6) Q(13) = Erosion during flood event only (Section 3.1)

(7) Q(15) = Deposition during flood events (Section 4)

6.4 Effect of Northern Jetty Construction

The foregoing equations and relationships were adjusted so as to

Fig-10 Karman vortex street formed by cloud behind Cheju Island (from Tsuchiya[1])

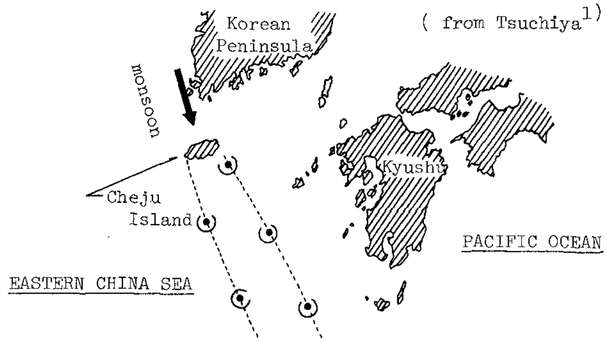

Table-1 Strength of vortices behind Cheju Island

Date	1969 Mar.05	1969 Mar.17	1969 Mar.22	1971 Jan.14	1971 Mar.13	
a km	36.8	44.0	61.3	48.8	35.4	
b km	110.8	71.0	86.1	121.8	76.2	
C m/sec	7.0	6.5	7.2	6.0	6.9	
U m/sec	9.2	10.5	12.0	8.3	10.5	
Γ_4 $10^9 m^2/sec$	6.3	5.9	8.4	6.6	6.1	←(eq. 5)
Γ_2 $10^9 m^2/sec$	6.7	6.0	8.6	7.0	6.1	←(eq. 3)
Γ_3 $10^9 m^2/sec$	10.2	7.5	10.3	10.1	8.0	←(eq. 4)

2-3 Strength of the Coherent Vortices in Naruto Strait

In order to estimate the strength of the coherent vortices in Naruto Strait, remote-sensing data from the airplanes were hydrodynamically interpreted using the above equations. On the Fig-7, one can estimate the surface concavity on the vortex axis to be $\Delta h = 1.0m$, the radius of the contourline of the concavity $\Delta h/2$ to be $R = 8m$. Putting these data into eq.(1), it is shown that the vortex strength amounts to about 160 m^2/sec, when the velocity of the tidal current is 8.2 knot. The space interval of the vortices b , and the shifting velocity C were measured on the aerophotos to get the results presented in Table-2, where the velocity of the tidal current U was gained from the onsite data, and the velocity in the dead water region was considered to be negligible. The strength of the vortices on the basis of eq.(3) is estimated to be 50∼100 m^2/sec in the case of the tidal flow velocity of 6.6 knots and 130∼200 m^2/sec in the case of 10 knots, respectively. The vortex strength gained by eq.(1), (3) and (4) is considered to agree well each other.

Table-2 Strength of the coherent vortices in Naruto Strait

(Vortex No. 1, 2, (1', 2',) means a vortex positioned in the right(left) hand free boundary layer ; X means distance between the numbered vortex and its generated point)

Date	Vortex No.	U m/sec	X m	b m	C m/sec	τ sec	Γ_2 m^2/sec	Γ_3 m^2/sec
1977 Apr. 1st	1	3.7	100	17	2.1	8	60	60
	2	-	120	28	3.1	9	60	100
	3	-	160	63	4.2	15	100	230
	4	-	240	90	3.8	24	160	330
	5	-	340	96	4.6	36	240	360
	6	-	440	163	4.0	41	280	600
	1'	-	170	73	3.5	21	140	270
	2'	-	240	74	2.9	25	270	170
	3'	-	320	66	2.1	32	220	250
	4'	-	380	86	3.3	26	180	320
	5'	-	490	129	4.6	28	190	480
	6'	-	630	143	4.2	34	230	530
1977 Jul. 2nd	1	4.1	150	80	3.9	21	170	330
	2	-	230	74	4.0	19	160	300
	3	-	300	66	3.5	19	160	270
	4	-	360	80	3.3	24	200	330
	5	-	460	96	4.5	21	180	390
1977 Mar. 8th	1	4.4	100	58	2.5	23	220	250
	2	-	160	59	3.4	17	170	260
	3	-	220	64	2.8	23	220	280
	4	-	290	73	2.5	29	280	320
	5	-	360	114	4.1	28	270	500
	1'	-	160	58	2.9	20	190	250
	2'	-	220	76	2.8	27	260	340
	3'	-	310	70	3.0	23	230	310
	4'	-	360	84	2.7	31	300	370
	5'	-	480	123	3.0	41	390	540
1978 Feb.24th	1	4.55	120	44	2.8	16	160	200
	2	-	160	52	4.2	12	130	240
	3	-	220	86	4.7	18	190	390
	4	-	340	82	3.3	25	260	370
	5	-	390	66	3.5	19	190	300
	6	-	470	100	4.0	25	260	460
	1'	-	280	56	4.0	14	140	250
	2'	-	340	50	3.2	16	160	230
	3'	-	380	48	2.8	17	180	220
	4'	-	430	76	3.4	23	230	350
	5'	-	530	100	5.3	19	200	450

2-4 Consideration of the Upwelling Current Associated with the Coherent Vortices

Onsite field observations and analysis of the solid aerophotos disclosed the existence of strong upwelling regions adjacent to the coherent vortices as shown in Fig-6. Theoretical considerations[2] using tornado-model show that a single line vortex around a vertical axis terminating at the sea surface and at the sea bottom, induces strong upward flow from the bottom due to the friction along the bed surface. Deducing from these results of a single line vortex, the observed upwelling phenomena at the strait are considered to be strictly related to the coherent vortices along the free boundary layer.

In order to estimate the upward volume flux in Naruto Strait, hydraulic model tests were carried. In a test basin of 0.6m-width and 25m-length, a single line vortex was generated by putting suddenly a plate of 0.3m-width into the uniform flow with the velocity of 7.0cm/sec, keeping it standing still in a moment, and finally drawing out abraptly. Both of the strength and diameter of the vortex could be changed by controling the degree of the small shifting motion of the plate toward the upstream. The vertical profiles of the water surface of the vortex were measured by a wave gauge set in the course of the vortex path. The vortex motion and the induced upwelling motion were coloured with respective different dyes and their side views as well as their plan views were photographed every one second. Experiments were carried under the two different conditions of bottom surface, that is, smooth surface and rough one with pasted sand of 1.7mm ~ 2.2mm diameter. The wave gauge was set at o.5m downstream from the vortex generating point. Experimental conditions are presented in Table-3, in which H is water depth, C is shifting velocity of the vortex and Γ is the vortex strength estimated by eq.(1) with the surface concavity gained by the wave gauge.

Case No.	1	2	3	4	5	6	7	8	9	10	11	12	13	14	15	16	17	18	19	20	21	22
Vortex velocity C (cm/sec)	7.7	8.0	7.2	7.5	5.5	8.3	8.0	8.3	7.0	5.6	7.7	7.0	8.2	7.2	7.8	7.5	7.8	8.0	8.2	8.0	7.9	6.8
Vortex radius a (cm)	2.08	3.60	3.02	3.82	3.96	1.62	2.28	2.74	3.36	3.19	3.28	2.31	2.58	3.67	4.21	1.91	3.28	3.36	4.18	3.12	2.61	3.57
Vortex concavity Δh (cm)	0.63	0.35	1.18	0.88	1.88	0.42	0.70	0.86	1.16	1.93	0.25	0.93	2.46	1.25	1.03	0.82	0.31	0.31	0.39	1.18	2.30	2.38
Vortex strength Γ (cm^2/sec)	325	419	645	705	1068	207	375	498	712	871	319	438	796	807	840	340	359	368	513	667	778	1038
Water depth H (cm)	20					20					30					30						
Bottom roughness	smooth					rough					smooth					rough						

Table-3 Experimental conditions

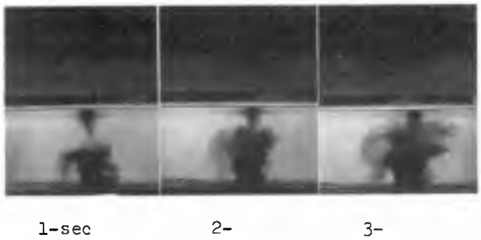

Fig-11

Upwelling due to a line vortex (Case 1)

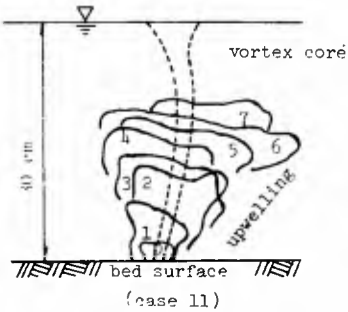

Fig-12

Successive picture of upwelling flow

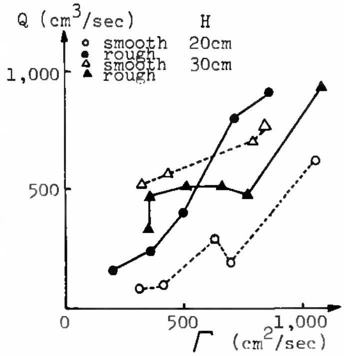

Fig-13

Upwelling flux as a function of vortex strength

When the vortex comes into the observation section, red colored dye set on the bottom surface moves along the bottom surface and turns its direction upward. In case of the vortices of weak strength, the upwelling flow concentrates near the vortex axis and breaks itself down before arriving at the water surface (Fig-11). According as the vortex strength increases, the downward flow along the vortex axis appears and increases its diameter, and the upwelling flow takes the shape of a ring. In the case of the rough bottom surface, the diameter of the upwelling flow becomes larger, and breaks down more easily because of the rotating energy consumption by the friction due to the bottom roughness.

Fig-12 shows the successive pictures of the upwelling flow mapped from a series of photos with the time interval of 1 sec. The upward volume flux associated with the upwelling motion was estimated from such figures gained respectively in each case of the experiments of Run 1～22 of Table-3. Fig-13 shows the relation of the upward volume flux to the vortex strength.

The upward volume flux at Naruto Strait was estimated by using these experimental data on the basis of the Froude similitude. In the experiments, the upward volume flux of $500cm^3/sec$ was observed to be induced by the vortex of 3cm-diameter, water surface concavity of 0.8cm and vortex strength of $500cm^2/sec$ in the case of water depth of 20cm. Basing on the Froude similitude, the upward volume flux of $280m^3/sec$ is expected to be induced by a vortex of 6m-diameter, 1.6m-concavity and $150m^2/sec$ strength in the case of water depth of 40m, which is of approximately equal scale to the coherent vortices in the free boundary layer generated at Naruto Strait in the flood tide condition. At Naruto, about a dozen of vortices are existing as shown in Fig-2, and then the total volume of upward flux is roughly estimated to be $3,000m^3/sec$. The total volume flux of the tidal current under the flood tide condition is about $100,000m^3/sec$. Therefore, at Naruto, the vertical sea water mixing caused by the upwelling motion induced by the coherent vortices is estimated to be a few percents of the total volume flux of the tidal current passing the strait.

3. LARGE SCALE VORTEX-PAIR OBSERVED BY LANDSAT

3-1 Remote-sensing by Landsat

As shown in Fig-4, the coherent vortices along the free boundary layers amalgamate into a pair of vortices of larger scale. This amalgamation phenomena have too large scale to observe from the airplane, but the satellite Landsat may present us these clearly. For example, Fig-14 shows a result of the analysis of the Landsat data obtained on August 1st. 1976. On this figure, one can see the vortex-pair of larger scale under the northward tidal current of the maximum velocity of 7.6 knot. Fig-15 is another example and shows the flow pattern on October 24th. 1972. In this case, the northward tidal flow maximum velocity of which is 10.2knot have just finished and the current is under the slack condition. The fully grown vortex-pair of large scale can be observed on this figure. Finally, Fig-16 obtained from the Landsat data on December 30th. 1975 shows the situation that the tidal current is flowing in the southward direction with about maximum velocity of 7.6knot while the vortex-pair left behind in the Harima Sea is still leaving away the strait with its self-induced velocity U_v , which is theoretically described by

$$U_v = \frac{\Gamma}{2\pi \ell} \tag{6}$$

where

Γ : strength of each vortex $= \alpha \int_0^{6hour} \frac{1}{2} u^2(t)\, dt$

ℓ : distance between each vortex

α : amalgamation efficiency factor

$u(t)$: velocity of the tidal current

Fig-14

Midst of the formation process at the maximum northward flow condition

Fig-15

Final stage of the formation process at the slack

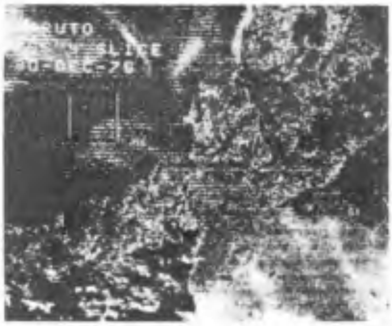

Fig-16

Vortex-pair progressing into the Harima Sea against surrounding sea water at the maximum southward flow condition

The above three different phases of large scale vortex-pair are summarized in the Fig-17. These Landsat data present clearly the various patterns of the vortex-pair formed by northward flow under each characteristic stage of the tidal cycle. On the other hand, patterns of vortex-pair formed by northward flow are not presented so clearly, although the vortex-pair can be vaguely recognized in Kii Channel in the case of Fig-16.

With the expectation to obtain more clear feature of the vortex-pair, the authors did measurements of thermal image of the flow from the airplane at the altitude of 4,000m. Fig-18 shows the thermal image gained at 11:00 A.M. Aug. 23rd 1979, being 2 hours after the southward flow began. Again the existence of the vortex-pair in the Harima Sea can be definitely recognized. Fig-19 shows the situation at 12:00 A.M. on the same date. The tidal condition at this moment is southward maximum flow. On this figure, one can see the vortex-pair in Kii Channel as expected and strong water mixing proceeding at the strait.

Fig-17

Three characteristic phases of the vortex-pair

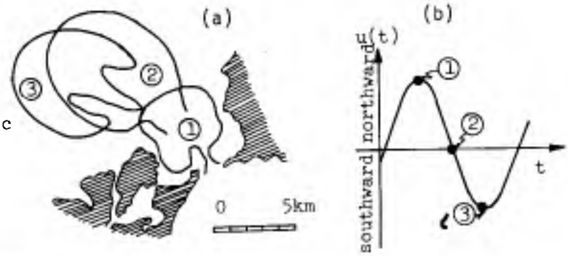

Fig-18 Thermal image at 11:00

Fig-19 Thermal image at 12:00

3-2 Consideration of Tidal-Exchange by Vortex-Pair

The mechanism of the tidal-exchange through the narrow strait such as Naruto Strait is explained using vortex-pair model as shown in Fig-20, in which A-①~③ represent the growing process of the vortex-pair, each of which corresponds to the typical phase of the cyclic tidal current at the strait as shown as B-①~③ .

① Tidal current is flowing with the maximum speed at the strait. The vortex-pair is being generated by the amalgamation process of the coherent vortices along the free boundary layer. At the same time, the vortex-pair advances forward with the self-induced propulsive force, pushing aside the surrounding water body.
② The first half of the tidal-cycle as well as the growing process of the vortex-pair are over.
③ Tidal current is running with the maximum speed in the reversal direction. Vortex-pair left behind is still leaving away the strait, with its self-induced velocity U_V defined by eq.(6) . Under this situation, the water mass passing the strait, which has been pushed aside by the vortex-pair in the former processes, generates another vortex-pair in the opposite side of the strait.

Thus tidal-exchange is inspired by the self-propelling motion of the vortex-pair.

The water mass forming the vortex pair corresponds to the magnitude of the tidal-exchange during one tidal cycle, which is estimated to be 10^9 m^3 in Naruto Strait as the result of the analysis of the remote-sensing data and onsite data as well. The self-propelling motion, which plays an important role in the tidal-exchange process through the strait, is also expected to contribute to the mixing process in the open seas neighboring the strait. Analyses of the remote-sensing data from Landsat show that the self-induced velocity of the vortex-pair at Naruto-Strait is about 0.8 knot, from which the strength of the vortex is estimated to be $10^4 m^2/sec$. Thus, about 10% of the vorticity generated at the strait is expected to amalgamate to the large scale vortex-pair via the form of the coherent vortices along the free boundary layer.

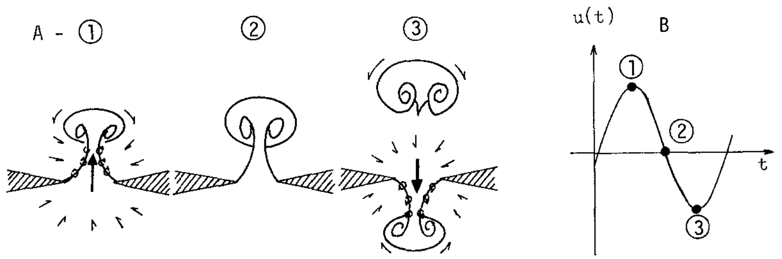

Fig-20 Schema of tidal-exchange mechanism

CONCLUSION

Usefulness of the remote-sensing from airplanes and Landsat in the study of tidal current in straits was discussed, choosing Naruto Strait as the object of the onsite study. Solid aerophoto provides various information of small scale hydrodynamical character of the tidal current including the distribution of the coherent vortices in the free boundary layer, surface concavity at the vortex axis and radius of the vortices, through which the strength of each coherent vortex can be estimated. Regarding the estimation of the vortex strength, the authors presented four formulas of eq.(1), (3), (4) and (5), of which fitness was studied by means of aerophotos. Among these, eq.(3) is considered to be most convenient in the case when we apply aerophotos in the study, because all variables in the equation can be obtained directly on the aerophotos.

The small scale coherent vortices amalgamate during a half of the tidal cycle, 6 hours, finally into a large scale vortex-pair, the self-propelling motion of which takes an important role in the tidal-exchange through the strait. The scale of the vortex-pair is generally too large to observe on the aerophotos. In that case, Landsat is quite useful as shown in Fig-14. The self-propelling motion of the vortex-pair is also considered to promote the mixing of the water from the inland sea with the water in the open sea. In the case of Naruto Strait, about 10% of the vorticity generated at the strait is expected to amalgamate in the vortex-pair via the form of small scale coherent vortices, and a few percents of total volume flux of the tidal current passing the strait is estimated to mix with the surrounding water body due to the upwelling current induced by the coherent vortices.

REFERENCES

1) Kiyoshi Tsuchiya (1974) : " Cloud Features Associated with Mesoscale Phenomena during Cold Season as Revealed by Meteorological Satellite Pictures", The Geographical Magazine, vol-37, No.1, pp49-94
2) Sotoaki Onishi and Tsukasa Nishimura (1979) : " Field Observations of Upwelling Associated with Vortex and Considerations of Generating Mechanism of These Phenomena", Coastal Engineering in Japan, vol-22 pp123-138